High-Resolution Imaging of Aromatic Molecules Adsorbed on Rh(111) and Pt(111) in Hydrofluoric Acid Solution: In Situ STM Study

Shueh-Lin Yau, Youn-Geun Kim, and Kingo Itaya*,†

Itaya Electrochemiscopy Project, ERATO/JRDC, Research Institute of Electric and Magnetic Materials, Yagiyama-Minami 2-1-1, Sendai 982, Japan

Received: December 3, 1996; In Final Form: February 19, 1997[⊗]

In situ scanning tunneling microscopy (STM) was employed to study adlayer structures of naphthalene, naphthoquinones, and anthracene on well-defined Rh(111) and Pt(111) electrodes in aqueous HF solutions. All molecules were adsorbed with the flat-lying orientation on both electrodes. Highly ordered adlayers of naphthalene and naphthoquinones were found to form on Rh(111) with the $(3\sqrt{3} \times 3\sqrt{3})R30°$ structure, while disordered structures were found on Pt(111). Anthracene formed almost close-packed adlayers without long-range ordering. In situ STM disclosed not only the adlayer structure and packing arrangement but also the internal structure of each aromatic molecule. Two- and three-ring structures were clearly discerned for naphthalene and anthracene, respectively. An additional spot was observed for 1,2-naphthoquinone, which was attributed to the oxygen atom at the 2-position.

Introduction

Scanning tunneling microscopy (STM) has been established as an invaluable in situ probe for the determination of structures of electrode−electrolyte interfaces with atomic resolution.[1,2] Particularly, adlayer structures of small inorganic species such as halide,[3−6] sulfate,[7−10] and cyanide,[11,12] adsorbed on well-defined single-crystal Pt, Rh, and Au electrodes have been directly determined by STM in solutions. STM has also made it possible to visualize organic molecules adsorbed on substrates.[13] Although adlayer structures of organic molecules have been intensively investigated in ultrahigh vacuum (UHV) using mainly low-energy electron diffraction (LEED),[14] STM in UHV recently disclosed packing arrangements and even shapes of various organic molecules such as benzene (on Pt(111)[15] and on Rh(111) with coadsorbed carbon monoxide[16]), naphthalene, and azulene on Pt(111)[17−19] and Cu phthalocyanine on Cu(100).[20] In the meantime, theoretical calculations were performed to derive models of the STM images of benzene molecules adsorbed on Pt(111),[21] and the results were found to agree qualitatively with the experimental observations.[15,16]

On the other hand, understanding the adsorption of organic molecules at electrode surfaces in electrolyte solution is one of the most important issues in elucidating the nature of electrode−electrolyte interfaces.[22] In contrast to a large number of successful results for imaging organic molecules in UHV, there has not been much success in electrolyte solutions under electrochemical conditions. However, recent efforts made it possible to visualize relatively simple molecules with high resolution in solutions. Examples include DNA bases[23] on graphite and Au(111),[23] xanthine and its oxidized form on Au(111),[24] porphyrins on graphite,[25] and 2,2′-bipyridine on Au(111).[26] Recently, we disclosed novel applications of iodine-modified electrodes as the substrates for the deposition of organic materials, which were found to facilitate direct visualization of organic molecules with near-atomic resolution.[27−29] Various iodine-modified electrodes of metals such as Au, Ag, Pt, and Rh were found to be suitable substrates on which to form highly ordered adlayers of relatively large organic molecules such as porphyrin and crystal violet.[30] In contrast, porphyrin forms a disordered adlayer on bare Au(111) electrode in the absence of an iodine monolayer.[31] This result clearly demonstrates that the interaction between molecules and substrates is an important factor in the processes of ordering of molecular adsorbates on substrates.

To understand the role of the interaction, we have recently used in situ STM to investigate the adlayer structures of benzene, the simplest aromatic molecule, chemisorbed on well-defined Rh(111) and Pt(111) electrodes in HF solutions.[32] Highly ordered benzene adlayers with $c(2\sqrt{3} \times 3)$*rect* and (3×3) structures were identified on Rh(111) in HF, depending on electrode potentials.[32] In addition to the $c(2\sqrt{3} \times 3)$*rect* structure, which was previously found in the absence of coadsorbed CO in UHV,[14,33] a different structure, $(\sqrt{19} \times \sqrt{19})$-*R*23.4°, was recently identified for a pure benzene adlayer on Rh(111) under "better" UHV conditions.[34] Although precise experimental conditions for the formation of these two structures in UHV have not been identified,[34] the $c(2\sqrt{3} \times 3)$*rect* structure was indeed observed in HF solution at positive potentials,[32] suggesting a similarity in the conditions of adsorbate−substrate interaction at the two interfaces. In contrast, although the degree of ordering of pure benzene adlayer on Pt(111) is known to be poor in UHV,[35] we discovered a well-ordered $(\sqrt{21} \times \sqrt{21})$-*R*10.9°structure on Pt(111) in HF solution, although it changed into a locally ordered $c(2\sqrt{3} \times 3)$*rect* structure located amid mostly disordered arrays at more positive potentials.[32] These results indicate that the nature of electrified interfaces can play an important role in the ordering processes of adsorbed organic molecules.

In this paper, we describe adlayer structures of larger aromatic molecules such as naphthalene, naphthoquinones, and anthracene formed on Rh(111) and Pt(111) in HF solutions. High-resolution in situ STM images allowed us to determine the adlayer structures, packing arrangements, and even internal structures of all of the aromatic molecules. The molecular shapes observed by in situ STM were consistent with corresponding molecular structures. The position of one of the two oxygen atoms in 1,2-naphthoquinone was discerned by STM. The surface diffusion of naphthalene molecules on Pt(111) was slow, resulting in the formation of a disordered phase.

† Faculty of Engineering, Tohoku University, Sendai 980, Japan.
⊗ Abstract published in *Advance ACS Abstracts,* March 15, 1997.

S1089-5647(96)03957-0 CCC: $14.00

Experimental Section

The Pt and Rh single-crystal beads were made by melting the ends of Pt and Rh wires (0.8 mm in diameter, Nalco Co.) in H_2-O_2 flame. The (111) facets formed on the single-crystal bead was used for STM measurements.[32] Mechanically exposed (111) surfaces were used for voltammetric measurements. The single-crystal electrodes were finally annealed in the flame and quenched in Millipore water. The flame annealing-and-quenching method produced large, atomically flat terraces,[4,11,32] which made it easy to determine adlayer structures in step-free areas. Prior to the injection of organic molecules, long-range ordered Rh(111) and Pt(111) surfaces with the (1×1) structure were discerned within the hydrogen adsorption−desorption and double-layer potential range between 0.1 and 0.6 V. To prevent the electrochemical reduction of naphthalene and anthracene, these molecules were introduced at a potential within the double-layer region. The 10 mM HF was made from *ultrapure* HF solution (27 M) from Cica-Merck (Darmstadt, FRG). The naphthalene and anthracene solutions were made from reagent-grade chemicals supplied by Kanto Chemical Co. (Tokyo, Japan), and they were used without further purification. All solutions were sonicated for more than 10 min to achieve saturation. The solubilities of benzene and naphthalene in water are known to be ca. 9 and 0.23 mM at room temperature, respectively.[36] Although the solubility of anthracene was expected to be very low, it was found in this study that the formation of a monolayer of anthracene was easily established in a saturated solution.

The STM used was a Nanoscope III (Digital Instruments, Santa Barbara, California). The W tips were prepared by a well-known procedure.[32] A potentiostat (Hokuto, Tokyo) was used to perform cyclic voltammetric measurements in a Teflon electrochemical cell equipped with a reversible hydrogen electrode (RHE) in 0.01 M HF and a Pt counter electrode. All electrode potentials are reported with respect to the RHE.

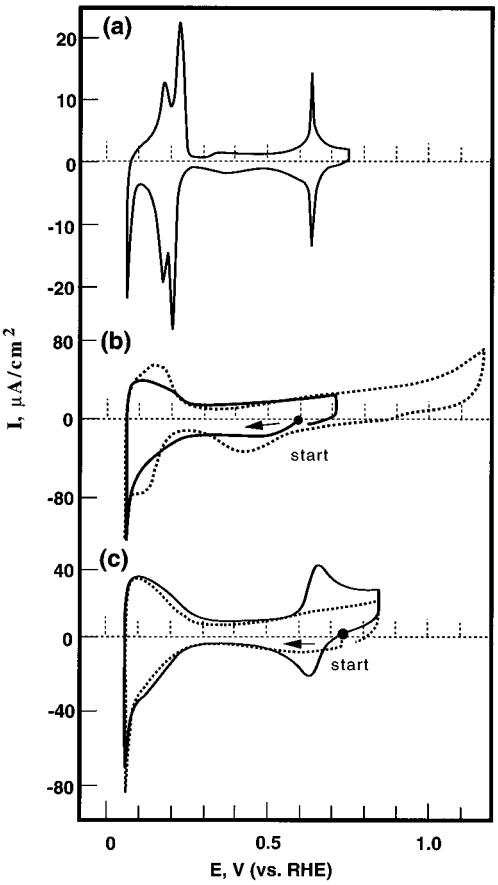

Figure 1. Cyclic voltammograms of a clean (a) and naphthalene-covered (b) Rh(111) electrode in 10 mM HF. The dotted line in (b) shows the CV of a roughened Rh(111) electrode. The solid and dotted traces in (c) were obtained with and without 1,2-naphthoquinone in the solution. The scan rates were 5 mV/s for (a) and 50 mV/s for (b) and (c).

Results and Discussion

Voltammetry. It has been shown that perchlorate anions can be electrochemically reduced on the Rh electrode, releasing chloride anions as a reduction product.[37,38] The chloride anions could be adsorbed on the Rh electrode as a contaminant, which complicates the study of adsorption of organic molecules. To avoid this problem, HF solution was exclusively used as in our previous study of the adsorption of benzene on a well-defined Rh(111) surface.[32] Figure 1a shows a typical cyclic voltammogram (CV) obtained on a well-defined Rh(111) in 0.01 M HF. Several highly symmetric peaks were observed. The so-called butterfly peaks and reversible doublet peaks were observed at ca. 0.6 and 0.15 V, respectively. The latter features with peaks at 0.15 and 0.18 V were observed only on well-prepared Rh(111) surfaces. The overall feature of the CV was almost identical with that reported in our previous paper,[32] indicating that CV can be used to diagnose the surface states of flame-annealed Rh(111) electrodes.

Such a well-defined Rh(111) electrode was transferred into 0.01 M HF containing organic molecules. Figures 1b shows the CV obtained in a naphthalene-saturated 0.01 M HF solution. The solid line was obtained in the limited potential window between 0.05 and 0.7 V. It is clear that the characteristic reversible peaks in Figure 1a disappeared almost completely in the solution containing naphthalene, leaving the featureless double-layer charging region between 0.3 and 0.7 V. This result indicates that a naphthalene adlayer blocks the hydrogen adsorption and desorption reactions as well as those involved in the butterfly peaks. The cathodic current commencing at 0.3 V might be partially due to the hydrogenation of naphthalene. The hydrogenation of benzene to cyclohexane is known to occur at cathodic potentials.[39] Similar results were obtained in an anthracene-saturated solution. The characteristic peaks observed on well-defined Pt(111) were also suppressed upon the adsorption of the molecules, as was found similarly for benzene.[32] The anodic current at potentials more positive than 0.7 V is due to the oxidation of the Rh(111) electrode superimposed on the oxidation of naphthalene. However, it was previously shown that the potential excursion up to 1.1 V, shown by the dashed line in Figure 1b, resulted in surface oxidation and roughening of the Rh(111) substrate.[40]

The presence of a monolayer of 1,2- and 1,4-naphthoquinone (NQ) on Rh(111) resulted in features in the CV similar to those of naphthalene. A well-defined Rh(111) electrode was immersed in the respective NQ-saturated solutions for 5 min, rinsed thoroughly with pure 0.01 M HF, and then transferred into the electrochemical cell containing 0.01 M HF in the absence of NQ. The dashed line shown in Figure 1c was recorded in the first potential cycle starting from 0.7 V for an adlayer of 1,2-NQ. On the other hand, the solid line was obtained in a solution containing 1,2-NQ (ca. 0.1 mM). The absence of clear surface redox peaks for the adsorbed 1,2-NQ suggests that it is electrochemically inactive, similar to hydroquinone adsorbed on Pt(111).[41] However, it was surprising that quasi-reversible peaks as shown by the solid line in Figure 1c appeared on Rh-(111) when the solution contained 1,2-NQ. These peaks are due to the redox reactions of naphthoquinone and corresponding hydroquinone in solution. Identical CV features were also

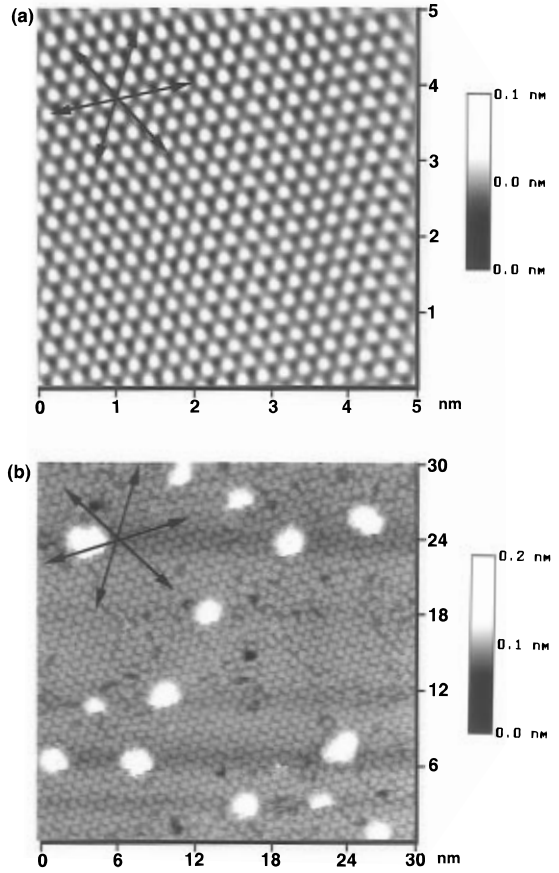

Figure 2. In situ STM images of Rh(111)-(1 × 1) (a) and a monolayer naphthalene on Rh(111) (b). These images were obtained at 0.3 V before and after the addition of naphthalene into the STM cell. The arrows show the close-packed directions of the Rh(111) substrate, which match those of the naphthalene adlattice.

observed with 1,4-NQ. Note that the result shown in Figure 1c is in strong contrast to the case of hydroquinone on Pt(111), where hydroquinone adlayers formed on Pt(111) were thought to act as an insulating layer to prohibit the electron-transfer reaction between the Pt electrode and hydroquinone in solution, resulting in very irreversible peaks.[41]

The CV results of Pt(111) in the presence of a naphthalene adlayer bear strong resemblance to those of Rh(111). However, in contrast to the documented CV results of benzene and aniline,[32,42] which exhibit very fine features near 0.1 V, only a sluggish increase of current as a function of potential was noted. Furthermore, repetitive potential cycling between 0.1 and 1.1 V completely removed surface naphthalene and restored the well-defined CV of Pt(111).

In Situ STM. *Naphthalene on Rh(111).* A well-prepared Rh(111) surface usually showed atomically flat terraces spanning over a few hundred nanometers as reported in our previous paper.[32] The atomic image of Rh(111)-(1 × 1) shown in Figure 2a was easily obtained on an atomically flat terrace in 10 mM HF solution in the potential range between 0.1 and 0.6 V. The almost perfectly aligned hexagonal structure can be seen with an interatomic distance of 0.27 nm. The close-packed directions, [110], of the Rh(111) substrate are indicated by the arrows shown in Figure 2a. It is clear that the atomic rows of Rh cross one another at either 60° or 120° within an experimental error of ±2°. This small distortion allowed us to determine the adlayer structure of naphthalene accurately.

After the atomic resolution shown in Figure 2a was achieved, a saturated naphthalene solution was added to the STM cell at 0.3 V. The averaged concentration of naphthalene was ca. 0.02

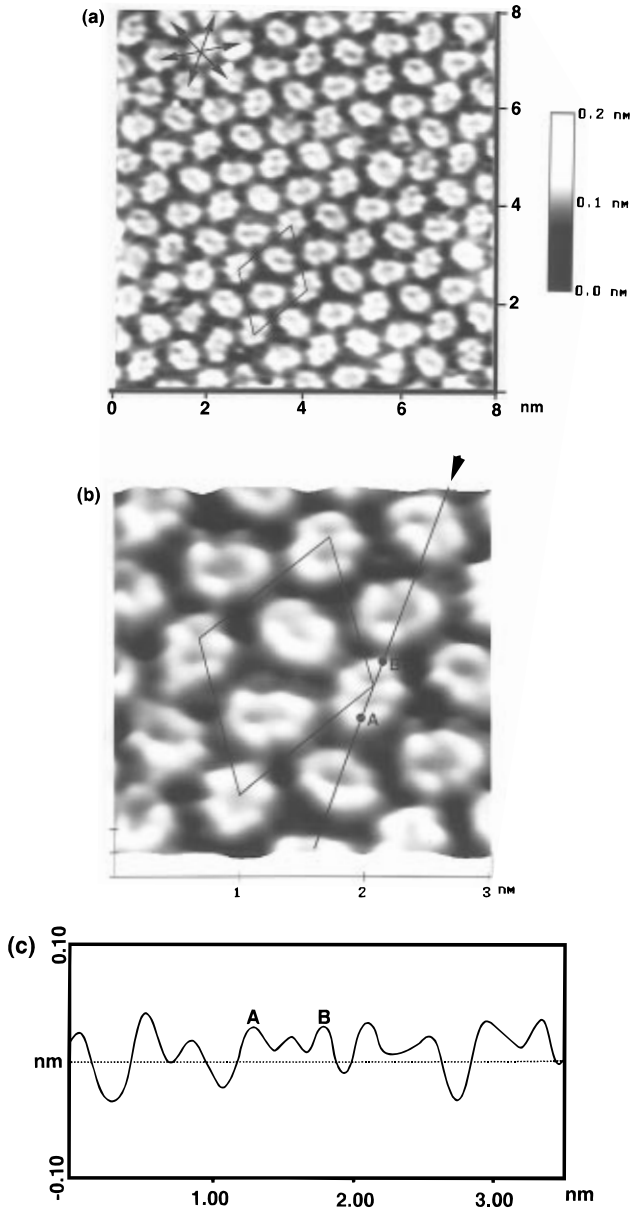

Figure 3. Close-ups (top view in (a) and perspective view in (b)) of the $(3\sqrt{3} \times 3\sqrt{3})R30°$-naphthalene adlayer on Rh(111). The rhombuses in (a) and (b) outline the unit mesh. The images were filtered with a 2D Fourier method to remove noise of less than 0.2 nm. The cross section profile in (c) reveals the corrugation along the line in (b). The width of a naphthalene molecule, as measured from point A to B in the figures, is 0.5 nm.

mM. Completely different patterns appeared in STM images within 10 min after the injection of naphthalene. Figure 2b shows a typical example of STM images, revealing a long-range ordered naphthalene adlayer. Some unidentified blotches exist amid the ordered molecular array. They might be molecular clusters of naphthalene or impurities. However, it is clearly seen in Figure 2b that the close-packed Rh atomic rows, pointed by the arrows in the figure, match the corresponding molecular rows of naphthalene.

A high-resolution image acquired in an ordered domain is shown in Figure 3a. It is more clearly seen that the molecular rows parallel the [110] directions of the substrate indicated by the arrows. More importantly, the STM image allowed us to determine the internal structure and orientation of each naphthalene molecule. The elongated features along the longer molecular axis (C_2) were discerned for each molecule. In addition, the images of some molecules clearly show a two-

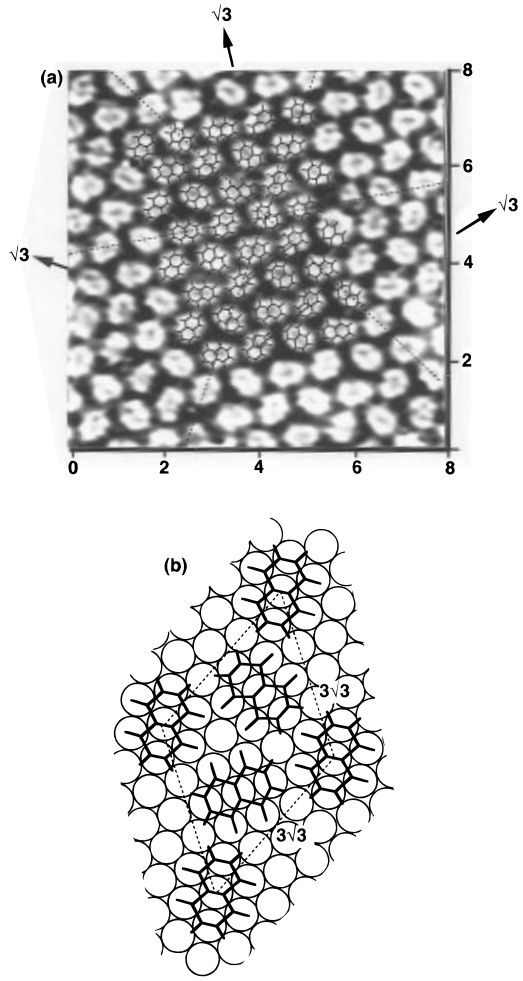

Figure 4. In situ STM images of the Rh(111)-(3√3 × 3√3)*R*30°-naphthalene structure with an overlaid molecular model (a). Note that all the molecules have the same orientation when viewed along the √3 direction. A ball model is presented in (b).

ring structure expected from the molecular model. It can also be seen that naphthalene molecules are perfectly aligned with a regular micro-orientation along the molecular rows. Periodical rotation of the molecules of naphthalene by 60° is seen within each molecular row with every third molecule being in the same orientation.

A further magnified view in height-shaded mode is shown in Figure 3b in which the two-ring structure can be more clearly seen. The nearest-neighbor distance of an average of 0.82 nm is equivalent to 3 times the Rh lattice of 0.268 nm. A corrugation profile along the line in Figure 3b is shown in Figure 3c, indicating two clearly distinguished dips of 0.01 nm in depth. The distance between two maxima, A and B along the C_2 axis, was ca. 0.5 nm, which is nearly consistent with the actual size of naphthalene molecule. However, a distance of 0.34 nm, found along the axis connecting the carbon atoms at the 1- and 4-positions, seems to be larger than the known value of 0.28 nm. This larger spacing might suggest that the hydrogen atoms attached to the 1- and 4-carbon atoms affect the appearance of naphthalene molecule in STM imaging.

According to the results described above, the unit cell can be defined by a (3√3 × 3√3)*R*30° symmetry as shown in Figure 3a. To make a comparison between the STM image and the adlayer structure, the STM image in Figure 3a is reproduced in Figure 4a with partially overlaid molecular models of naphthalene. This (3√3 × 3√3)*R*30°structure results in a surface coverage of 0.11. A ball model of this structure is illustrated in Figure 4b. It is now clear that all naphthalene molecules align their C_2 axes along the close-packed directions of the Rh substrate. The molecules aligned along the [112] directions, the so-called √3 directions, have the same orientation. The spacing between two adjacent molecules along the √3 direction is measured to be 1.4 nm, which is 3 times the √3 spacing. In the model structure shown in Figure 4b, two carbon atoms at the 9- and 10-positions are assumed to be attached directly to a Rh atom. It is noteworthy that this structure is identical with that previously proposed from LEED results by UHV workers.[43] If one recalls the identical results for benzene adsorbed on Rh(111) in UHV and in HF solution,[32] it can be stated that the results of naphthalene further support the predominant adsorbate−substrate interaction for hydrophobic molecules and the minor role of water molecules. It must be noted, however, that the (3 × 3)-benzene structure on Rh(111) in UHV results from coadsorption of CO,[16] which is in contrast to the possible coadsorption of water molecules or hydronium cations at the electrified interfaces.[32]

Naphthalene on Pt(111). A typical arrangement of naphthalene molecules on Pt(111) at 0.3 V is represented by the STM image shown in Figure 5a, revealing a full monolayer of flat-lying naphthalene molecules. Some unidentified blotches were also frequently found on the naphthalene adlayer, which were thought to be coadsorbed impurities or molecular clusters. Although the overall appearance of the naphthalene adlayer on Pt(111) in the large scale is similar to that on Rh(111), shown in Figure 3b, close inspection reveals that the adlayer includes many randomly oriented molecules. Because the molecular rows are nearly parallel to the close-packed Pt atomic rows and because the intermolecular distance is 3 times that of the Pt substrate, this structure roughly fits a (3 × 3) symmetry.

To describe the arrangement of naphthalene in greater detail, a close-up view of the outlined square in Figure 5a is displayed in Figure 5b in which the close-packed directions of Pt(111) determined by an STM image of Pt(111)-(1 × 1) are indicated by the arrows. A corresponding ball model for Figure 5b is presented in Figure 5c. Similar to the case of Rh(111), the center of each naphthalene molecule is assumed to lie on an on-top site, and it is oriented with its long C_2 axis in parallel with the close-packed directions of *a*, *b*, and *c*. The bilobe appearance resembling that observed in UHV[18] is indicative of its molecular orientation. More details of the molecular arrangements are revealed by viewing along the directions indicated by arrows I and II in parts b and c of Figure 5. An ideally ordered (3√3 × 3√3)*R*30° naphthalene structure, as was found on Rh(111), would have been formed on Pt(111) if the molecules continuously rotated by 60°, as indicated by A, B, and C along the molecular row of I. However, most molecules did not follow this pattern. For example, naphthalene only rotated alternatively between *a* and *b* orientations in the direction of II. Evidently, intermolecular interaction was not strong enough to force naphthalene molecules to adapt specific orientations. For example, two nearest neighbors sometimes adapted the same orientation along a molecular row, as indicated by A and A′ in Figure 5b. This type of configuration is associated with the formation of domain boundaries, which is also noted by UHV workers.[18] With the aid of the dashed line in Figure 5b, it can be seen that A′ is shifted sideways by a distance equal to the lattice constant with respect to A.

We have previously demonstrated that the surface diffusion of adsorbed molecules played an important role in the formation of well-ordered adlayers.[32] We anticipated that naphthalene molecules were more strongly adsorbed on Pt(111) than on Rh-(111), resulting in a lower diffusion rate and thus a disordered phase. Once naphthalene molecules land on the surface, they

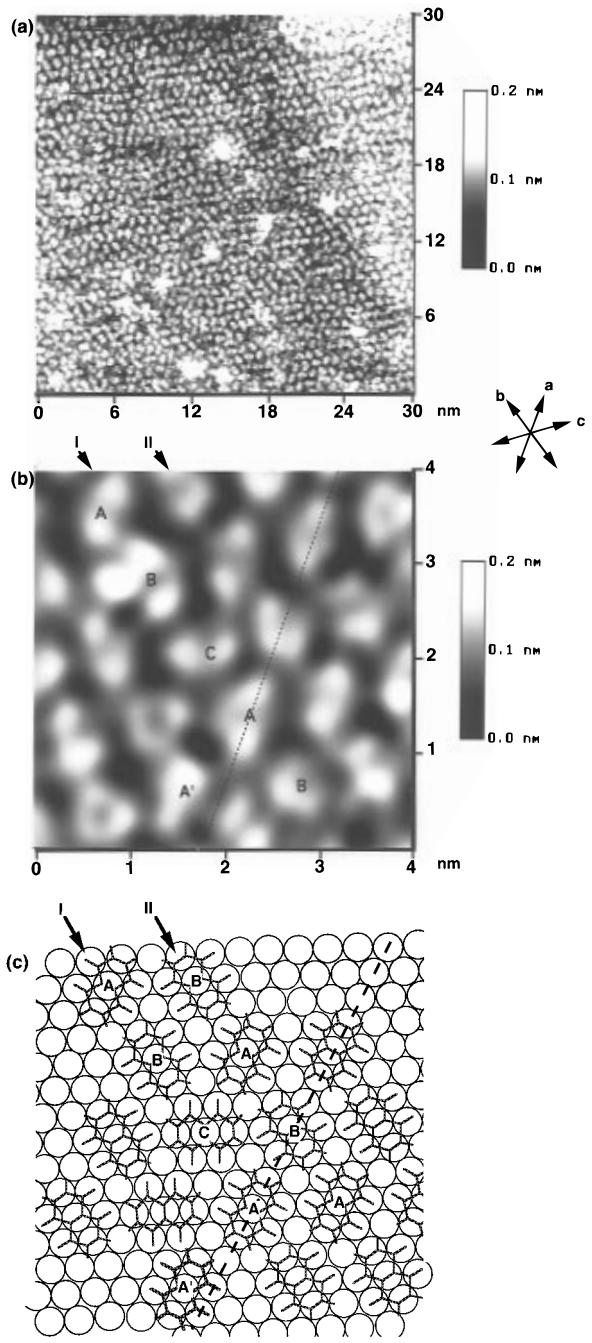

Figure 5. In situ STM images of naphthalene adsorbed on Pt(111) where (b) highlights the inscribed square in (a). Two naphthalene molecules, labeled A and A′, exhibit an end-to-end configuration. The ball model in (c) outlines the arrangement of naphthalene in (b). The arrows show the close-packed directions of the Pt(111) substrate.

are unlikely to diffuse and even reorient themselves to create an ordered pattern. This point can be further illustrated by a separate experiment in which isolated naphthalene molecules on Pt(111) were clearly discerned. After acquisition of the image shown in Figure 5a, the solution containing naphthalene was completely replaced by a pure HF solution. A similar disordered structure was also observed in the pure HF solution at 0.3 V, indicating that the molecules are strongly attached to Pt(111). It was found in this study that a potential excursion to 0.1 V led to partial desorption of naphthalene, as previously found for benzene.[32] The typical image shown in Figure 6 surprisingly reveals the internal structure of naphthalene molecule with two craters 0.03 nm deep. It is more clearly seen that all molecules align their C_2 axes along the close-packed directions of the Pt substrate. In addition, it was found that the

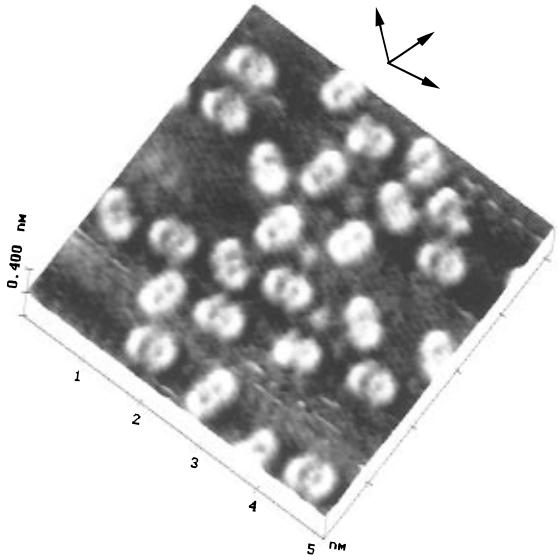

Figure 6. In situ STM image showing the packing arrangement of a submonolayer naphthalene on Pt(111). The image was obtained at 0.1 V.

molecules were immobile on Pt(111) even at such a low surface coverage. Identical images with the same orientation were consistently observed for at least 15−20 min, indicating that the surface diffusion of naphthalene on Pt(111) is very slow. For this reason, the degree of ordering was not improved by prolonged exposure or potential cycles between 0.1 and 0.8 V in solutions containing naphthalene. A similar experiment was carried out for the naphthalene adlayer on Rh(111) in the pure HF solution. Although naphthalene adsorbed on Rh(111) were largely immobile, notable movement was observed for isolated naphthalene molecules. This comparatively high mobility of naphthalene on Rh(111) is partly responsible for its formation of a long-range ordered adlayer, which did not form on Pt-(111) at room temperature.

Naphthoquinone. We have briefly investigated 1,2- and 1,4-naphthoquinone (NQ) as representative derivatives of naphthalene in order to understand the effect of functional groups on the molecular organization. Generally speaking, these quinones, similar to naphthalene, formed ordered adlayers on Rh(111) and mostly disordered adlayers with the flat-lying orientation on Pt-(111). Typical STM images of 1,2-naphthoquinone are shown in Figure 7. In contrast to the result obtained with naphthalene in Figure 3a, many unidentified bright small spots and blotches appeared over an ordered molecular array. The high-resolution STM image shown in Figure 7b further reveals the details of internal molecular structures. The superimposed adlayer structure on the image clearly demonstrates that 1,2-naphthoquinone formed a well-ordered adlayer with the identical structure, $(3\sqrt{3} \times 3\sqrt{3})R30°$, identical with that found for naphthalene. This assignment does not include the consideration of features resulting from the presence of oxygen atoms in the molecules because these features do not form a well-ordered pattern. Note that the arrows in Figure 7 represent the close-packed directions of Rh. However, it is interesting to note that an additional bright spot, unseen in the image for naphthalene, is seen at the 2-position of each 1,2-naphthoquinone molecule. This spot exhibits ca. 0.03 nm higher corrugation with respect to the naphthalene ring, which is likely to be due to the oxygen at the 2-position. The oxygen at the 1-position was not clearly seen in the STM images. The different appearances of the oxygen atoms at the two different positions can be explained by their different registries. If the same adlayer structure as that shown in Figure 4b is assumed to form for 1,2-naphthoquinone, it can

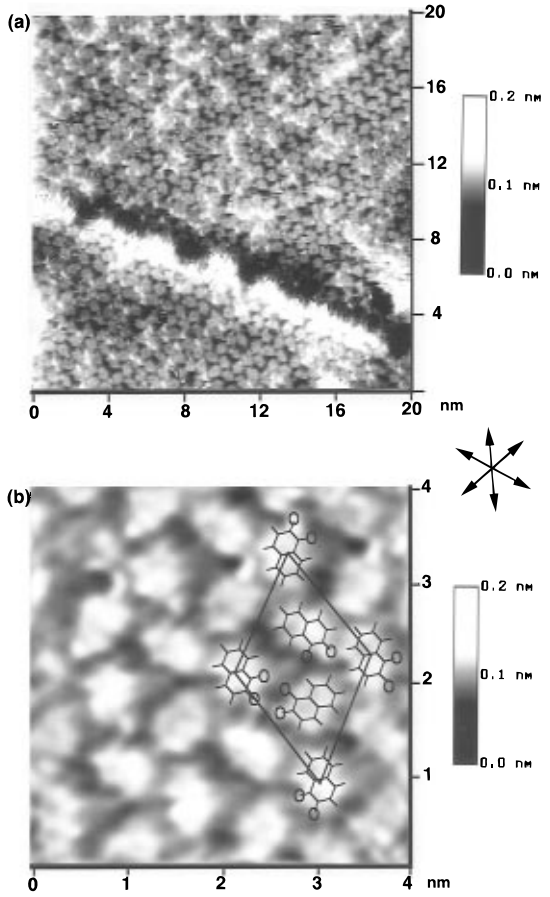

Figure 7. In situ STM images of 1,2-naphthoquinone on Rh(111). The close-up view in (b) highlights the ordered structure of $(3\sqrt{3} \times 3\sqrt{3})R30°$, as revealed by the superimposed molecular models and a rhombus.

be expected that the two oxygen atoms at the 1- and 2-positions occupy on-top and 2-fold bridge sites, respectively. It is well-known that the appearance of adatoms in STM images with atomic resolution depends on their registries, imaging conditions, and molecular orbitals. Typically, adatoms at the on-top sites give rise to the largest corrugation height in the STM image, followed by those at 2-fold and 3-fold sites, as was first reported for iodine atoms adsorbed on Pt(111).[44] However, the appearance of oxygen adatoms on metal surfaces in the STM atomic resolution may not follow this rule of thumb. For example, some UHV−STM studies of oxygen adsorption on Ni and Al reported a depressed appearance of 4-fold oxygen adatoms on Ni(100).[45] In the present case, the 2-fold oxygen atom appears to be bright and the on-top one is essentially invisible. According to the CV behavior shown in Figure 1c, these oxygen atoms might not be reduced even at 0.4 V, which is in agreement with the previous ex situ UHV−electrochemical study of hydroquinone on Pt(111).[41] It is also important to note that STM images of 1,4-naphthoquinone did not show additional spots corresponding to the oxygen atoms at the 1- and 4-positions, which also supports our interpretation described above. More detailed studies for quinones are now in progress.

Anthracene. The in situ STM image reproduced in Figure 8a shows a monolayer for anthracene on Rh(111) with clear resolution for each individual molecule. A close-up view of Figure 8a is shown in Figure 8b, revealing preferential alignment of the molecules with their long C_2 axis along the close-packed directions of Rh, which was also observed for naphthalene. Once again, the orientations of the Rh(111) substrate, as indicated by the arrows in the figure, can be checked easily by in situ STM imaging at 0.1 V. The STM image in Figure 8b was

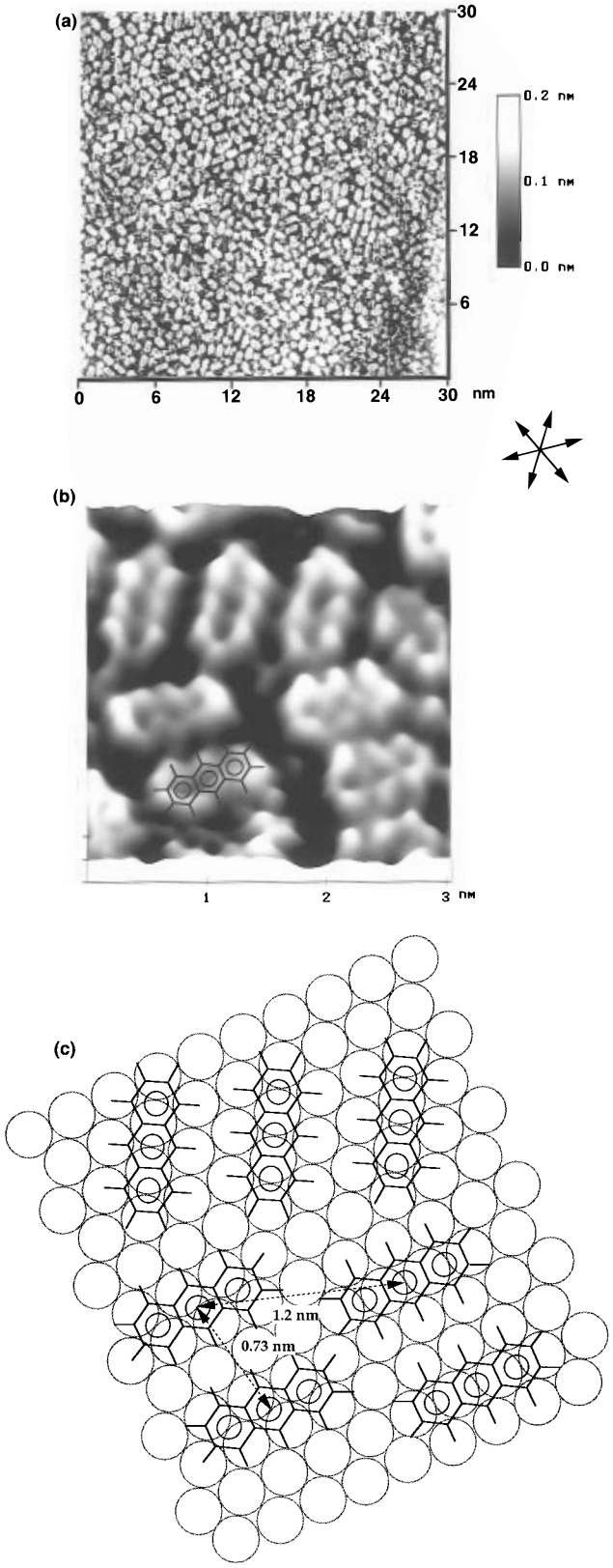

Figure 8. In situ STM images of a full monolayer of anthracene on Rh(111). The image was acquired at 0.3 V with a bias voltage of 100 mV and 30 nA. The higher resolution scan in (b) reveals the internal molecular structures of anthracene. A corresponding molecular structure is presented in (c).

filtered by a 2D FT method to remove features of less than 0.2 nm. This result unambiguously discloses the internal molecular structure of anthracene with clear identification of three craters in each molecule. The length and width of a single anthracene molecule are 0.8 and 0.35 nm, respectively, and its corrugation

of 0.08 nm is comparable to the values for benzene and naphthalene imaged in UHV or in solution.[16,18,32] Molecules of anthraquinone and 1,4,9,10-anthracenetetrol, although not shown here, also adsorbed in a similar manner.

The real space structure of anthracene can be extrapolated from that of naphthalene. Despite the lack of ordering, one can readily visualize the adsorption of anthracene by appending one more aromatic ring to the naphthalene molecule. A real-space ball model is depicted in Figure 8c, which corresponds to the STM result in Figure 8b. Note that all the anthracene molecules align with their long C_2 axes with the close-packed directions of Rh and that all three aromatic units within each molecule occupy 2-fold bridge sites. Two anthracene molecules adapt an end-to-end configuration, but they must compensate for the intermolecular repulsion by shifting to the next neighboring atomic row. The closest spacings of 0.73 and 1.2 nm can be found in the anthracene adlayer as indicated in the figure. We have also examined the adsorption of anthraquinone and 1,4,9,10-anthracenetetrol on Rh(111), and similar results were obtained. The lack of 2D ordering of these anthracene derivatives is tentatively attributed to the strong adsorbate−substrate interaction, as was discussed for the case of naphthalene on Pt(111).

Conclusion

In situ STM allowed visualization of the arrangements of naphthalene, naphthoquinone, and anthracene molecules adsorbed on Rh(111) and Pt(111) in 10 mM HF. On Rh(111) naphthalene and naphthoquinone yielded a long-range ordered $(3\sqrt{3} \times 3\sqrt{3})R30°$ structure, whereas anthracene produced a disordered structure. On Pt(111) disordered structures were formed with naphthalene and naphthoquinone, whereas anthracene yielded nearly close-packed adlayers without long-range ordering. They maintain their molecular symmetry while maximizing the number of coordination to the hexagonal substrates by adsorbing in a way such that the molecules were centered above a Rh or Pt atom with their aromatic rings at 2-fold bridge sites. The results demonstrate that high-quality STM images with atomic resolution provide direct information on coordination of adsorbed molecules to atoms of metallic substrates. In this study such STM images clearly revealed the internal molecular structures of the polycyclic aromatic compounds adsorbed on Rh(111) and Pt(111).

Acknowledgment. This work has been supported by ERATO/JST. The authors also thank Dr. Y. Okinaka for his help in editing the manuscript.

References and Notes

(1) Siegenthaler, H. In *Scanning Tunneling Microscopy II*; Wiesendanger, R., Guntherodt, H.-J., Eds.; Springer-Verlag, Berlin, 1992; pp 7−49.
(2) Bard, A. J.; Abruna, H. D.; Chidsey, C. E.; Faulkner, L. R.; Feldberg, S. W.; Itaya, K.; Majda, M.; Merloy, O.; Murray, R. W.; Porter, M. D.; Soriaga, M. P.; White, H. S. *J. Phys. Chem.* **1993**, *97*, 7147.
(3) Yau, S.-L.; Vitus, C. M.; Schardt, B. C. *J. Am. Chem. Soc.* **1990**, *112*, 3677.
(4) Tanaka, S.; Yau, S.-L.; Itaya, K. *J. Electroanal. Chem.* **1995**, *396*, 125.
(5) Gao, X. P.; Weaver, M. J. *J. Am. Chem. Soc.* **1992**, *114*, 8544.
(6) Yamada, T.; Batina, N.; Itaya, K. *J. Phys. Chem.* **1995**, *99*, 8817.
(7) Magnussen, O. M.; Hagebock, J.; Hotlos, J.; Behm, R. J. *Faraday Discuss. Chem. Soc.* **1992**, *94*, 329, 398.
(8) Funtikov, A. M.; Linke, U.; Stimming, U.; Vogel, R. *Surf. Sci.* **1995**, *324*, L343.
(9) Wan, L-J.; Yau, S-L.; Itaya, K. *J. Phys. Chem.* **1995**, *99*, 9507.
(10) Edens, G. J.; Gao, X.; Weaver, M. J. *J. Electroanal. Chem.* **1994**, *375*, 357.
(11) Kim, Y.-G.; Yau, S.-L.; Itaya, K. *J. Am. Chem. Soc.* **1996**, *118*, 393.
(12) Stuhlmann, C.; Villegas, I.; Weaver, M. J. *Chem. Phys. Lett.* **1994**, *219*, 319.
(13) Chiang, S. In *Scanning Tunneling Microscopy I*; Wiesendanger, R., Guntherodt, H.-J.; Eds.; Springer-Verlag: Berlin, 1991; pp 181−205.
(14) Somorji, G. A. *Introduction to Surface Chemistry and Catalysis*; John Wiley & Sons: New York, 1993.
(15) Weiss, P. S.; Eigler, D. M. *Phys. Rev. Lett.* **1993**, *71*, 3139.
(16) Ohtani, H.; Wilson, R. J.; Chiang, S.; Mate, C. M. *Phys. Rev. Lett.* **1988**, *60*, 2398.
(17) Hallmark, V. M.; Chiang, S.; Woll, Ch. *J. Vac. Sci. Technol.* **1991**, *9*, 1111.
(18) Hallmark, V. M.; Chiang, S.; Brown, J. K.; Woll, Ch. *Phys. Rev. Lett.* **1991**, *66*, 48.
(19) Hallmark, V. M.; Chiang, S.; Meinhardt, K. P.; Hafner, K. *Phys. Rev. Lett.* **1993**, *70*, 3740.
(20) Lippel, P. H.; Wilson, R. J.; Miller, M. D.; Chiang, S. *Phys. Rev. Lett.* **1989**, *62*, 171.
(21) Sautet, P.; Bocquet, M.-L. *Phys. Rev. B* **1996**, *53* (8), 4910.
(22) Lipkowski, J., Ross, P. N., Eds. *Adsorption of Molecules at Metal Electrodes*; VCH Publishers: New York, 1992.
(23) Tao, N. J.; DeRose, J. A.; Linday, S. M. *J. Phys. Chem.* **1993**, *97*, 910.
(24) Tao, N. J.; Shi, Z. *J. Phys. Chem.* **1994**, *98*, 1464.
(25) Tao, N. J.; Cardenas, G.; Cunha, F.; Shi, Z. *Langmuir* **1995**, *11*, 4445.
(26) Cunha, F.; Tao, N. J. *Phys. Rev. Lett.* **1995**, *75*, 2376.
(27) Kunitake, M.; Batina, N.; Itaya, K. *Langmuir* **1995,** *11*, 2337.
(28) Batina, N.; Kunitake, M.; Itaya K. *J. Electroanal. Chem.* **1996**, *405*, 245.
(29) Ogaki, K.; Batina, N.; Kunitake, M.; Itaya, K. *J. Phys. Chem.* **1996**, *100*, 7185.
(30) Itaya, K.; Batina, N.; Kunitake, M.; Ogaki, K.; Kim, Y.-G.; Wan, L.-J.; Yamada, T. In *Electron Spectroscopy and STM/AFM Analysis of the Solid−Liquid Interface*; Jerkiewicz, G., Wieckowski, A., Uosaki, K., Soriaga, M. P., Eds.; American Chemical Society: Washington, DC, in press.
(31) Kunitake, M.; Akiba, U.; Batina, N.; Itaya, K. *Langmuir*, submitted.
(32) Yau, S. L.; Kim, Y. G.; Itaya, K. *J. Am. Chem. Soc.* **1996**, *118*, 7795.
(33) Mate, C. M.; Somorjai, G. A. *Surf. Sci.* **1985**, *160*, 542.
(34) Neuber, M.; Schneider, F.; Zubragel, C.; Newman, M. *J. Phys. Chem.* **1995**, *99*, 9160.
(35) Wander, A.; Held, G.; Hwang, R. Q.; Blackman, G. S.; Xu, M. L.; Andres, P.; Van Hove, M. A.; Somorjai, G. A. *Surf. Sci.* **1991**, *249*, 21.
(36) Dean, J. A., Ed. *Lange's Handbook of Chemistry*; McGraw-Hill: New York, 1985.
(37) Rhee, C. K.; Wasberg, M.; Zelenay, P.; Wieckowski, A. *Catal. Lett.* **1991**, *10*, 149.
(38) Clavilier, J.; Wasberg, M.; Petit, M.; Klein, L. H. *J. Electroanal. Chem.* **1994**. *374*, 123.
(39) Baltruschat, H.; Schmiemann, U. *Ber. Bunsen-Ges. Phys. Chem.* **1993**, *97*, 452.
(40) Wan, L.-J.; Yau, S.-L.; Swain, G. M.; Itaya, K. *J. Electroanal. Chem.* **1995,** *381*, 105.
(41) Lu, F.; Salaita, G.; Laguren-Davidson, L.: Stern, D.; Wellner, E.; Frank, D.; Batina, N.; Zapien, D. C.; Walton, N.; Hubbard, A. T. *Langmuir* **1988**, *4*, 637.
(42) Albalat, R.; Claret, J.; Feliu, J. M.; Clavilier, J. *J. Electroanal. Chem.* **1990**, *288*, 277.
(43) Lin, R. F.; Koestner, R. J.; VanHove, M. A.; Somorjai, G. A. *Surf. Sci.* **1983**, *134*, 161.
(44) Schardt, B. C.; Yau, S. L.; Rinaldi, F. *Science* **1989**, *243*, 1050.
(45) Kopatzki, E.; Behm, R. J. *Surf. Sci.* **1991**, *245*, 255.